First near-threshold measurements of the $^{13}C(\alpha, n_1)^{16}O$ reaction for low-background-environment characterization

R. J. deBoer,[1,*] A. Gula,[1] M. Febbraro,[2] K. Brandenburg,[3] C. R. Brune,[3] J. Görres,[1] Gy. Gyürky,[4] R. Kelmar,[1] K. Manukyan,[1] Z. Meisel,[3] D. Odell,[3] M. T. Pigni,[2] Shahina,[1] E. Stech,[1] W. Tan,[1] and M. Wiescher[1]

[1]*Department of Physics and Astronomy, University of Notre Dame, Notre Dame, Indiana 46556, USA*

[2]*Oak Ridge National Laboratory, Oak Ridge, Tennessee 37830, USA*

[3]*Department of Physics and Astronomy, Ohio University, Athens, Ohio 45701, USA*

[4]*Institute for Nuclear Research (Atomki), P.O.B. 51, H-4001 Debrecen, Hungary*

(Received 3 September 2022; accepted 7 November 2022; published 21 November 2022)

The modeling of background sources in large volume detection systems requires accurate nuclear cross sections for a variety of reactions. Among the most important are (α, n) on light nuclei, where α particles, up to ≈9 MeV, are produced from the decay of actinides present in trace amounts in detection and structural material. In order to model the neutron energy spectra and production of other secondary particles, the partial cross sections are needed. Yet very little experimental data exists for these partial cross sections because past measurements, hampered by the experimental challenges of neutron detection, have focused mostly on total reaction cross section measurements. Here the partial cross section of the $^{13}C(\alpha, n_1)^{16}O$ reaction is reported for the first time. The measurements were made near the reaction threshold using a high energy resolution helium spectrometer. The measurements show a rapidly increasing cross section, which quickly becomes a significant fraction of the total reaction cross section. Measurements are compared with previous theory estimates and differences of more than an order of magnitude are found. A comparison is made with new total cross section measurements and the current level of consistency is demonstrated.

DOI: 10.1103/PhysRevC.106.055808

I. INTRODUCTION

Dark matter, neutrino, and neutrinoless double β decay measurements all require very-low-background, deep-underground environments in order to achieve unprecedented levels of sensitivity. Under these conditions, the background signals induced by cosmic rays that are encountered in surface laboratories are greatly suppressed, yet backgrounds from the decay of naturally occurring radioactive isotopes in the surrounding rock and structural materials remain and are often even larger than on the Earth's surface. Energetic α particles, up to ≈9 MeV, are produced from actinide decays, which in turn can undergo (α, n) reactions on light elements that are also often present in significant amounts due to their high natural abundances. The reaction that often produces the highest yield is $^{13}C(\alpha, n)^{16}O$ ($Q = +2.2$ MeV), producing neutrons up to ≈11 MeV, sometimes in coincidence with γ rays and β particles [1–9].

Simulations of these neutron background sources are often very critical in the design stage of large volume detector experiments, as they determine the amount of shielding that will be needed. Thus inaccurate or poor precision measurements can directly translate into inflated construction costs. Yet measurements are often only available for part of the energy ranges required or, worse, do not exist at all. In addition, the partial cross section data that are truly needed to accurately reproduce the neutron energy spectrum when multiple final states are energetically accessible are almost never available. This fact can be easily overlooked by end users, since simulation software very often does not include uncertainties on the input cross sections taken from evaluations, giving simulations a false sense of confidence and causing confusion when source measurements do not match simulation. Most simulations rely on a single evaluation for (α, n) reactions, the JENDL/AN-2005 data set [10], where statistical model calculations are often used when experimental data are unavailable. While this is a common practice, because there is no better alternative, these model calculations carry with them large uncertainties, especially for light nuclear systems, which are often not clearly indicated.

Recently, Febbraro *et al.* [11] showed that insufficient information about the different partial cross sections for the $^{13}C(\alpha, n)^{16}O$ reaction could have a significant impact on the background estimation for a portion of the neutrino data obtained at KamLAND that was used to determine ν_1–ν_2 mixing [12]. In that work, it was emphasized that the $^{13}C(\alpha, n_1)^{16}O$ partial cross section was of particular importance, because it results in the simultaneous emission of a neutron and a positron, which can mimic inverse β decay ($p + \bar{\nu}_e \rightarrow n + e^+$).

In this work, measurements of the low energy cross section of the $^{13}C(\alpha, n_1)^{16}O$ reaction are reported for the first time. The measurements cover the low energy range from the reaction threshold near $E_\alpha = 5$ MeV up to 5.6 MeV. Because of experimental constraints, most of the present measurements

*rdeboer1@nd.edu

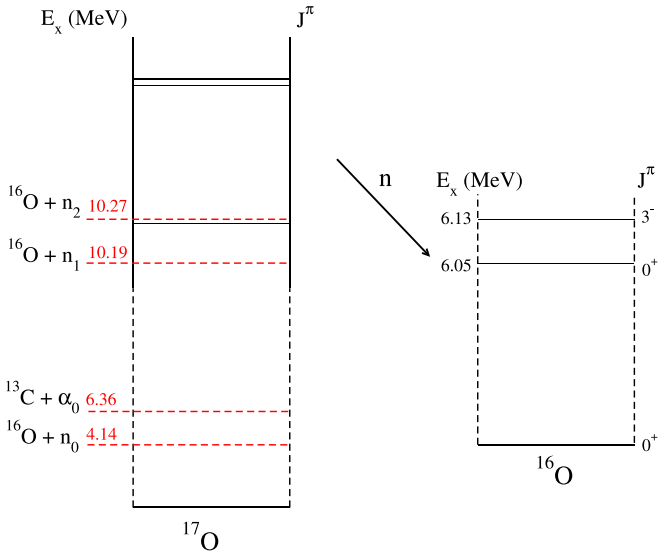

FIG. 1. Simplified level diagram of the ^{17}O system [13] over the region of the present experimental measurements.

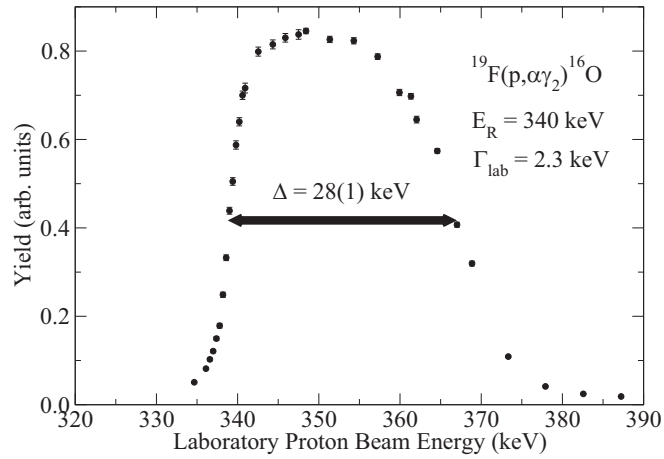

FIG. 2. Thick target yield curve of the $E_p = 340$ keV resonance in the ^{19}F$(p, \alpha\gamma)^{16}$O reaction used to obtain the thickness of the LiF calibration target

are limited to a differential excitation curve at a single forward angle of $\theta_{\text{lab}} = 15^\circ$, but angular distribution measurements are performed at few select energies. The data are analyzed using a simplified *R*-matrix analysis, which was used to make a rough estimate of the angle integrated cross section. Using ^{13}C$(\alpha, n_0)^{16}$O and ^{13}C$(\alpha, n_2)^{16}$O measurements from other studies, a comparison is made with recent total cross section measurements to estimate the level of consistency. A simplified level diagram of the ^{17}O system is given in Fig. 1.

Section II describes the experimental setup and the conversion from experimental yields to differential cross sections is described in Sec. III. Section IV details the *R*-matrix analysis used to estimate the angle integrated cross section from differential measurements, and further discussions are presented in Sec. V. Summarizing remarks are given in Sec. VI.

II. EXPERIMENTAL SETUP

Experimental measurements were performed at the University of Notre Dame Nuclear Science Laboratory (NSL). The Stable ion Accelerator for Nuclear Astrophysics (Sta. ANA) 5 MV accelerator was used to produce a He^{++} beam covering a laboratory energy from $E_\alpha = 5.0$ to 5.57 MeV and a proton beam of $E_p = 0.34$ to 3 MeV. Beam intensities from 5 to 20 μA and from 1 to 6 μA were impinged on target for the α-particle and proton beams, respectively. Beam-stop targets, all with identical 0.5 mm thick Ta backings, were mounted on a low-mass, electrically isolated, water cooled, aluminum target holder. A 1 inch diameter electrically isolated copper pipe was mounted inside the beam pipe just upstream of the target. The pipe was both cooled with liquid nitrogen and biased to -300 V in order to act as both a cold trap and electron suppressor.

Carbon targets were produced at the Institute for Nuclear Research (ATOMKI) in Debrecen, Hungary. Enriched (99%) ^{13}C powder was evaporated onto a 0.5 mm Ta backing, creating a thin layered target of $\approx$10 μg/cm^2 ($\approx 7 \times 10^{17}$ atoms/cm^2) nominal thickness. A precise target thickness was determined by comparing neutron yields from the present target with that of Brune *et al.* [14], where the target thickness of Brune *et al.* [14] was determined to 10% uncertainty using Rutherford backscattering. The yield ratio measurements for the different targets were performed at the Edwards Accelerator Laboratory at Ohio University [15] using the HeBGB long counter [16]. Measurements were made at a relatively constant region of the cross section at $E_\alpha = 2.9$ MeV. The target thickness, found by normalizing to the yield of the target from Brune *et al.* [14], was found to be $6.8(7) \times 10^{17}$ atoms/cm^2, in good agreement with the nominal value.

LiF targets of natural isotopic abundance were also utilized for the efficiency calibration of the neutron detector using the ^{7}Li$(p, n)^7$Be reaction. The LiF material was evaporated onto 0.5 mm thick Ta backings using an evaporator setup at the NSL. The target thickness was determined by performing a thick-target scan of the narrow ($\Gamma \approx 2$ keV) $E_p = 340$ keV resonance in the ^{19}F$(p, \alpha\gamma_2)^{16}$O reaction using a $CeBr_3$ detector for the measurement of 6.13 MeV γ rays, as shown in Fig. 2. The number of Li atoms in the target was determined assuming a 1:1 isotopic composition of Li and F and stopping powers from the code SRIM [17]. The proton energy loss observed through the target was observed to be $\Delta = 28(1)$ keV, giving, after considering the natural abundance of lithium isotopes, a target thickness of $3.2(2) \times 10^{18}$ ^{7}Li atoms/cm^2.

The detection setup consisted of a single ^{3}He spectrometer (FNS-100, Bubble Technology Industries [18]) mounted on a rotating swing arm to enable angular distribution measurements between $0 < \theta_{\text{lab}} < 135^\circ$. The swing arm was supported by a large table, which was machined to accurately indicate the angle of rotation. Because of the detector geometry, water cooling, and the desire to make well defined angular measurements, the detector was positioned far from the target. This resulted in a low detection efficiency, but provided a straightforward geometry that facilitated the conversion of the experimental yields into absolute differential cross sections.

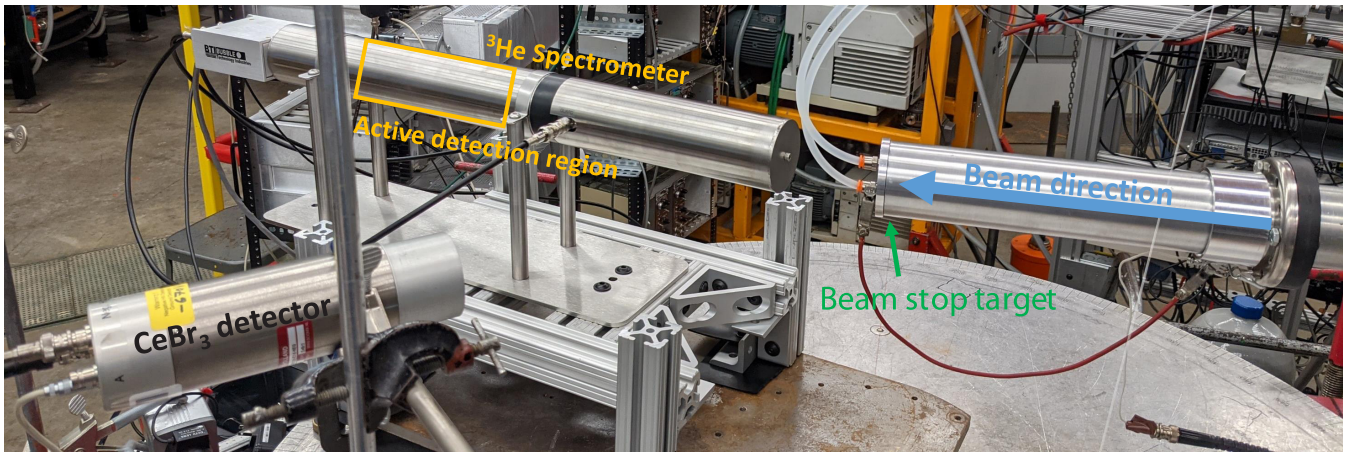

FIG. 3. Experimental setup. The ^{3}He spectrometer was mounted on a rotatable swing arm, which could be moved between $\theta_{lab} = 0$ and 135°. A $CeBr_3$ detector was mounted at $\theta_{lab} = 45°$ to monitor secondary γ rays.

The setup is shown in Fig. 3. The analog electronics, for both the ^{3}He spectrometer and $CeBr_3$ detector, consisted of an ORTEC 672 spectroscopic amplifier and a Canberra 8715 analog-to-digital converter. Signals from both detectors were fed into a four-channel FAST MPA-3 multichannel analyzer.

III. DATA ANALYSIS

A sample spectrum from the ^{3}He spectrometer is shown in Fig. 4. An energy resolution for the thermal peak of less than 20 keV was obtained and that of the reaction peaks was ≈30 keV, which are typical for this detector type [18]. The spectrum is free from background peaks from other reactions, e.g., $^{19}F(\alpha, n)^{22}Ne$, but there is a significant, nearly constant background present from high energy ground state neutrons from the $^{13}C(\alpha, n_0)^{16}O$ reaction. This background is the result of the continuum created by incomplete energy loss of these high energy neutrons in the active counter volume ("wall effects") [19]. Since the ground state cross section is always significant over this energy range, this constant background is always present, hindering measurements of the $^{13}C(\alpha, n_1)^{16}O$ cross section, especially in off-resonance regions.

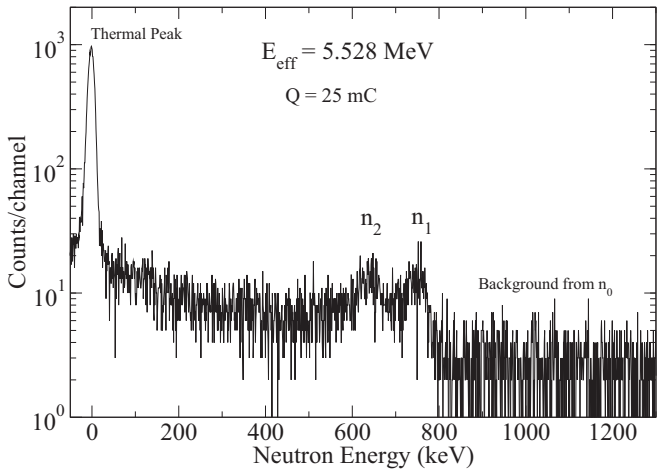

FIG. 4. Neutron energy spectrum in the ^{3}He spectrometer for an evaporated ^{13}C target on a Ta backing at $E_{eff} = 5.528$ MeV. Neutron peaks corresponding to the $^{13}C(\alpha, n_1)^{16}O$ and $^{13}C(\alpha, n_2)^{16}O$ reactions are resolved. The flat background is primarily the result of the much larger Q-value $^{13}C(\alpha, n_0)^{16}O$ reaction.

Further, at the highest energies investigated, appreciable yields were observed for the $^{13}C(\alpha, n_2)^{16}O$ reaction. As this reaction has a Q value that is only ≈80 keV less than the $^{13}C(\alpha, n_1)^{16}O$ reaction, high energy resolution was critical. This was the main reason a ^{3}He spectrometer was utilized for this measurement, despite its very low efficiency.

The absolute cross sections for the present $^{13}C(\alpha, n_1)^{16}O$ measurements were determined through normalization to the $^7Li(p, n)^7Be$ differential cross sections of Burke *et al.* [20], which were available in digital form in the EXFOR database [21]. Due to the low efficiency of the setup and the instability of LiF targets under high current beam bombardment, calibration measurements were made at only a few sample energies. This still provided an accurate determination of the efficiency, since the shape was well characterized previously [19]. Facilitating the analysis, a functional representation of the efficiency shape is available in Ohm *et al.* [22]. The absolute efficiency of the ^{3}He spectrometer is shown in Fig. 5.

From the ^{13}C target thickness and the absolute efficiency, the $^{13}C(\alpha, n_1)^{16}O$ differential cross sections were determined. A thin target approximation was assumed as the observed resonance structures were wide compared to the beam energy loss through the target, which was approximately constant ($\Delta E \approx 8$ keV). The effective energy was determined as $E_{eff} = E_{beam} - \Delta E/2$.

The majority of the experimental measurements were made at $\theta_{lab} = 15°$ due to experimental constraints. This small forward angle was chosen instead of 0° to avoid attenuation from the water cooling lines. The laboratory differential cross section for the $^{13}C(\alpha, n_1)^{16}O$ reaction at $\theta_{lab} = 15°$ is shown in Fig. 6. Angular distribution measurements were made at four energies as indicated in Fig. 7. Table I summarizes the uncertainty contributions to the cross section measurements. The data are provided in the Supplemental Material [23].

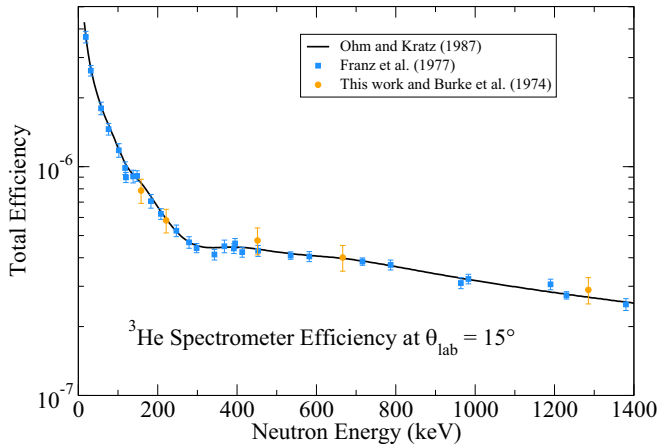

FIG. 5. The absolute detection efficiency of the ^{3}He spectrometer in the geometry shown in Fig. 3. The efficiency was determined by normalizing the differential yield measurements of the ^{7}Li$(p, n)^7$Be reaction to the differential cross section data of Burke *et al.* [20] and was interpolated using the efficiency function of Ohm *et al.* [22] that was produced from the experimental data of Franz *et al.* [19].

IV. SINGLE REACTION *R*-MATRIX ANALYSIS

In order to estimate the angle integrated cross section, a simplified *R*-matrix calculation was performed using the code AZURE2 [25,26] and the uncertainty was estimated using the Bayesian *R*-matrix Inference Code Kit (BRICK) [27]. The fit was done using the alternative *R*-matrix parametrization of Brune [28], and channel radii of $a_\alpha = 6.684$ fm and $a_{n_0} = a_{n_1} = 4.15$ fm. Several previous *R*-matrix fits exist for the ^{17}O system (e.g., Heil *et al.* [24], Leal *et al.* [29], Chakraborty

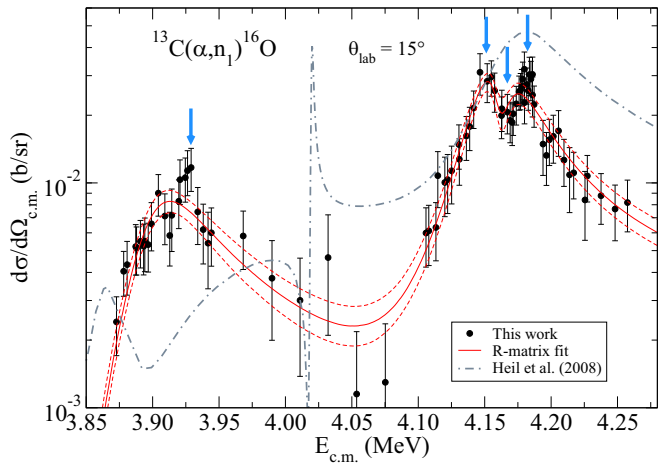

FIG. 6. The laboratory differential cross section of the ^{13}C$(\alpha, n_1)^{16}$O reaction at $\theta_{lab} = 15°$. The indicated uncertainties result only from statistics. The blue vertical arrows indicate energies where angular distributions were measured. The dashed-dotted grey line represents an *R*-matrix calculation of the differential cross section performed with SAMMY using the parameters of Heil *et al.* [24]. The red solid and dashed lines indicate the cross section and uncertainty (68% confidence limits), respectively, of the *R*-matrix fit of this work.

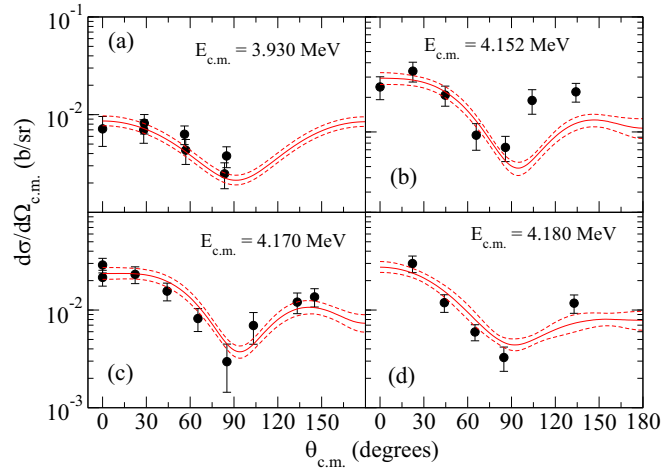

FIG. 7. Angular distribution measurements for the ^{13}C$(\alpha, n_1)^{16}$O reaction.

et al. [30], and that found in the ENDF/B-VIII.0 evaluation [31]), but due to the lack of higher energy data, they, for the most part, are limited to lower energies than the present data. The fit of Heil *et al.* [24] does extend into and above the range of the current data, but it was found that the ^{13}C$(\alpha, n_1)^{16}$O cross section calculated from the parameters of that work did not accurately describe the present data as shown in Fig. 6.

The data indicated at least three resonances in the ^{13}C$(\alpha, n_1)^{16}$O reaction, over the region of measurement (see Fig. 6). Angular distributions were measured near the maxima of the three resonances as shown in Fig. 7. The large cross sections on top of the resonances, the close proximity to the threshold, and the Wigner limits of the reduced width amplitudes likely limit these resonances to corresponding levels that can be populated in the exit channel with relative orbital angular momentum $\leqslant 2$. Table II summarizes the *R*-matrix fit parameters that were found to give a good description of the experimental data, but it should be noted that, due to the limited nature of the fitting, the fit is not unique.

V. DISCUSSION

As these are the first measurements of the ^{13}C$(\alpha, n_1)^{16}$O cross section, there are no previous data to directly compare with. Estimates of the cross section have been made in the JENDL-AN evaluation [10], the global *R*-matrix fit of Heil

TABLE I. Summary of systematic uncertainty estimates.

Systematic uncertainty contribution	(%)
^{13}C target thickness	10
LiF target thickness	3.6
^{7}Li$(p, n)^7$Be cross section [20]	5
Efficiency function [19]	3
Target degradation	10
Beam current reading	3
Total	16

TABLE II. *R*-matrix level parameters in the Brune parametrization [28]. Channel radii of 4.150 and 6.684 fm were used for the neutron and α-particle partitions respectively. Masses and separation energies were taken from the AME 2016 mass evaluation [32,33]. Uncertainties in the widths were calculated using the Markov chain Monte Carlo routine EMCEE [34], implemented for the AZURE2 code using the Python package BRICK [27]. Negative signs on the partial widths indicate the sign of the corresponding reduced width amplitude. The dominant uncertainties in the level energies corresponds to the systematic uncertainty in the energy calibration of accelerator.

$E_{\text{c.m.}}$(MeV)	E_x (MeV)		J^π		Γ_{n_0} (keV)	Γ_{α_0} (keV)	Γ_{n_1} (keV)	Γ (keV)	
This work	This work	[13]	This work	[13]		This work		This work	[13]
		10.240		$7/2^+$					122
3.904(8)	10.263(8)		$(3/2^-)$			$62.1^{+7.1}_{-6.5}$	$11.5^{+2.2}_{-1.6}$	$74^{+8.5}_{-7.7}$	
		10.335(15)		$(5/2^+, 7/2^-)$					155
		10421.3(20)		$(5/2^-, 7/2^-)$					14(3)
4.154(8)	10.513(8)		$(5/2^+)$		$2.8^{+4.0}_{-1.9}$	$19.6^{+5.6}_{-5.8}$	$19.5^{+7.0}_{-6.4}$	42^{+15}_{-14}	
4.165(8)	10.524(8)	10.5	$(5/2^+)$	$(5/2^+, 7/2^-)$	$-19.8^{+7.1}_{-6.7}$	$8.5^{+5.3}_{-4.1}$	$31.0^{+11.6}_{-14.9}$	59^{+22}_{-28}	75(30)
4.168(8)	10.527(8)	10.5623(8)	$(5/2^+)$	$(7/2^-)$	$8.8^{+6.0}_{-5.2}$	$19.8^{+16.7}_{-8.5}$	$5.3^{+2.4}_{-1.8}$	34^{+29}_{-15}	44.5(25)

et al. [24], and more recently by Mohr [35]. The JENDL-AN [10] and Mohr [35] estimates rely heavily on statistical model calculations (MEXIFON [36] and TALYS [37], respectively). The statistical model was used to calculate the branching ratios of the different final state transitions and these were then applied to the reaction cross section measurements of Bair and Haas [38] and Harissopulos *et al.* [39], respectively. These calculations should only be expected to give very rough estimates of the partial cross sections, since in this region resonances are still clearly resolved. Further, the uncertainty in these calculations is difficult to estimate, often resulting in no uncertainty being given.

This point is highlighted in Fig. 8, where the *R*-matrix estimate of the cross section from the present experimental results is compared to the statistical model calculations of JENDL-AN [10] and Mohr [35] and a previous comprehensive *R*-matrix fit by Heil *et al.* [24]. Different calculations vary from one another by approximately an order of magnitude.

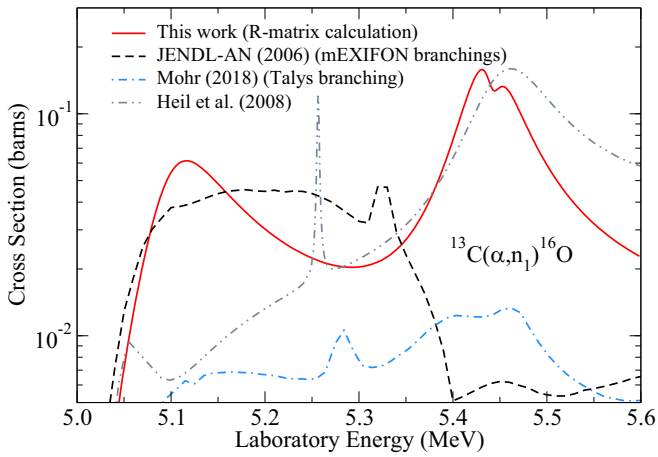

FIG. 8. Comparison of the $^{13}\text{C}(\alpha, n_1)^{16}\text{O}$ partial cross section of this work (red solid line) with previous theoretical estimates from the JENDL-AN evaluation [10] (black dashed line) and by Mohr [35] (blue-dashed-dotted line) using the branching ratios from the statistical codes MEXIFON [36] and TALYS [37], respectively. The global *R*-matrix fit of Heil *et al.* [24] is indicated by the grey dashed-dotted-dotted line.

Close to the reaction threshold, the theoretical calculations from JENDL-AN are in reasonable agreement with the present data, but at higher energies, above $E_\alpha \approx 5.4$ MeV, the JENDL-AN calculation underestimates the cross section substantially. In contrast, the *R*-matrix calculation of Heil *et al.* [24] is in better agreement over the higher energy region, but underestimates the cross section at low energies. In addition, the calculation of Heil *et al.* [24] predicts a strong narrow resonance at $E_\alpha \approx 5.25$ MeV, which does not appear, at least as strongly, in the present $^{13}\text{C}(\alpha, n_1)^{16}\text{O}$ data. This resonance instead appears strongly in the $^{13}\text{C}(\alpha, n_2\gamma)^{16}\text{O}$ cross section [11,40,41]. The cross section calculated from Mohr [35] underestimates the cross section over the entire range.

The compilation [13] reports five levels in the energy region covered by the present data ($10.21 < E_x < 10.59$ MeV). The first level is at $E_x = 10.240$ MeV (no quoted uncertainty) and has a J^π assignment of $7/2^+$. Because of the penetrability, it is very unlikely that this level corresponds to the broad resonance observed in the present data at $E_x = 10.263(8)$ MeV, so close to the n_1 separation energy ($S_{n_1} = 9.448$ MeV), as it would have to be populated through $\ell = 4$ in the n_1 exit channel. The next level is located at $E_x = 10.335(15)$ MeV and has tentative J^π assignments of $5/2^+$ or $7/2^-$. This level could also correspond to the near threshold level observed here at $E_x = 10.263(8)$ MeV, but again, even with $\ell = 2$, it is unlikely due to the n_1 penetrability. The reported width is also significantly larger than that observed here. The next level at $E_x = 10.4213(20)$ MeV has too small of a width to correspond to any of the levels observed here, but likely corresponds to the narrow resonance observed strongly in the n_2 channel. The level at $E_x = 10.5$ MeV (no uncertainty given) could correspond to either of the levels observed here at $E_x = 10.524(8)$ or $10.527(8)$ MeV and the J^π assignment of $5/2^+$ (exit channel $\ell = 2$) is consistent with he measured angular distributions and penetrability. Its reported total width, 75(30) keV, is also similar to that found here, 59^{+22}_{-28} keV. Finally, the level at $E_x = 10.5623(8)$ MeV is very close in energy to the highest energy level observed in the present study at $E_x = 10.527(8)$ keV, and the widths are similar, 44.5(25) and 34^{+29}_{-15} keV respectively. However, the level in the compilation has $J^\pi = (7/2^-)$, which again would be unlikely due to penetrability, but this assignment is tentative. Given the above

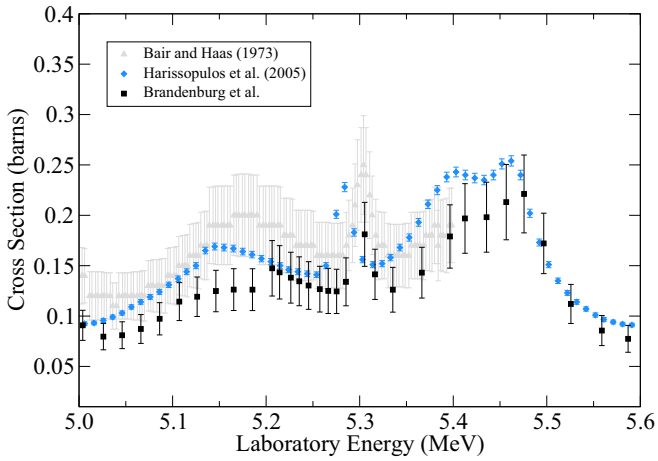

FIG. 9. Comparison of the $^{13}C(\alpha, n)^{16}O$ reaction data of Bair and Haas [38], Harissopulos *et al.* [39], and Brandenburg *et al.* [43].

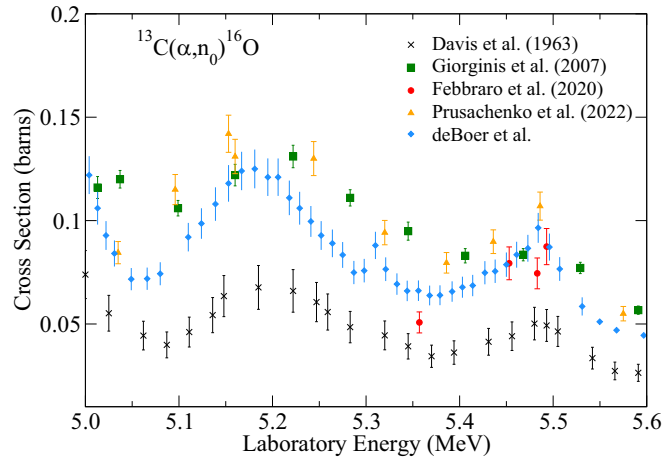

FIG. 10. Comparison of the $^{13}C(\alpha, n_0)^{16}O$ data of Febbraro *et al.* [11], Prusachenko *et al.* [44], and deBoer *et al.* [45], as well as the inverse data of Davis *et al.* [46] and Giorginis *et al.* [47].

considerations, the two highest energy resonances observed in the present study likely correspond to previously observed levels in other reactions but the lower energy two do not. The levels observed here are compared with those from the compilation in Table II. A multichannel *R*-matrix analysis that takes into account all previously existing data could likely yield more definitive results, but that is beyond the scope of the current work.

The present $^{13}C(\alpha, n_1)^{16}O$ partial cross section data can be summed together with other partial cross section data and compared with total reaction cross section data to check for consistency. This calculation is somewhat complicated by problems with past $^{13}C(\alpha, n)^{16}O$ reaction data [35,42], especially that of Harissopulos *et al.* [39]. Recently, a new measurement of the $^{13}C(\alpha, n)^{16}O$ reaction cross section was made [43] with improved accuracy by using a neutron moderator detector with a much more constant efficiency and where angular distribution effects were also corrected. The difference in the cross section is significant over the region of the present data, showing not just a difference in overall normalization, but also in shape, as shown in Fig. 9.

For the $^{13}C(\alpha, n_0)^{16}O$ cross section, measurements have been made over this energy by Febbraro *et al.* [11], Prusachenko *et al.* [44], and deBoer *et al.* [45] and using the inverse reaction by Davis *et al.* [46] and Giorginis *et al.* [47] as shown in Fig. 10. The shape of the $^{13}C(\alpha, n_0)^{16}O$ cross section is fairly consistent among the different measurements, but the overall scale varies by a factor of ≈2.

Measurements of the $^{13}C(\alpha, n_2)^{16}O$ cross section have been reported only as differential measurements of the secondary γ ray by Spear *et al.* [41], Febbraro *et al.* [11], and deBoer *et al.* [40]. The different measurements are compared in Fig. 11. The measurements of Spear *et al.* [41] can be compared directly with those of deBoer *et al.* [40], as they were made at the same angle. The data of Spear *et al.* [41] show a higher cross section in the off-resonance regions, with the discrepancy increasing at lower energies. This is attributed to incomplete background subtraction in that measurement, where a low resolution sodium iodide detector was used, compared to the high-purity germanium detector detector used by deBoer *et al.* [40].

Given the above considerations, the $^{13}C(\alpha, n_0)^{16}O$ data of deBoer *et al.* [45] and the $^{13}C(\alpha, n_2)^{16}O$ data of deBoer *et al.* [40] have been combined with the $^{13}C(\alpha, n_1)^{16}O$ data of this work to compare with the $^{13}C(\alpha, n)^{16}O$ reaction cross section measurements of Brandenburg *et al.* [43], as shown in Fig. 12. In the data shown, only the point-to-point uncertainties are indicted in the plot, while the systematic uncertainties dominate for the different reactions, these being 16% for the present $^{13}C(\alpha, n_1)^{16}O$ data, 10% for the $^{13}C(\alpha, n_2\gamma)^{16}O$ data of deBoer *et al.* [40], and 13% for the $^{13}C(\alpha, n_0)^{16}O$ data of deBoer *et al.* [45]. The $^{13}C(\alpha, n_1)^{16}O$ cross section begins to make a significant contribution very close to the reaction threshold at ≈5.0 MeV, rising rapidly and becoming nearly equal in magnitude to the $^{13}C(\alpha, n_0)^{16}O$ cross section data of deBoer *et al.* [45] at ≈5.1 MeV. The sum of these partial cross sections somewhat overestimates the reaction cross section of Brandenburg *et al.* [43] below $E_\alpha \approx 5.2$ MeV, but at higher

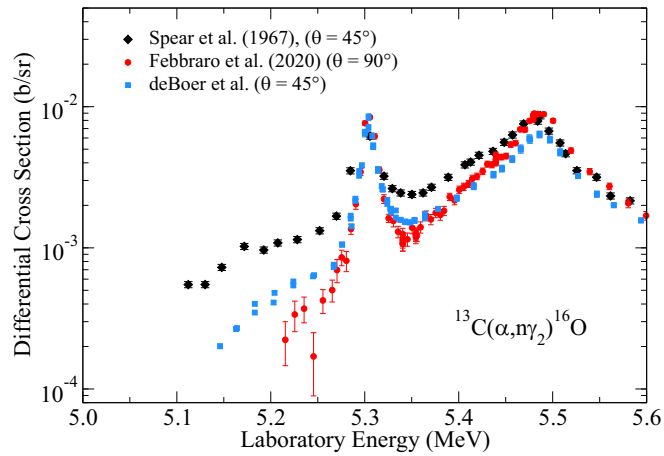

FIG. 11. Comparison of the $^{13}C(\alpha, n_2)^{16}O$ data of Spear *et al.* [41], Febbraro *et al.* [11], and deBoer *et al.* [40].

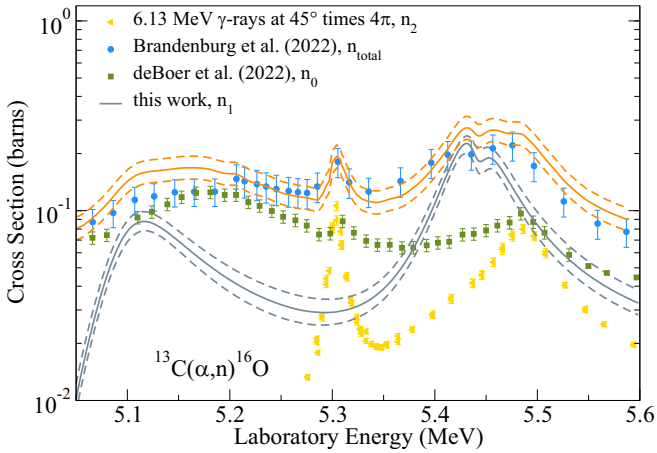

FIG. 12. Comparison of the total $^{13}C(\alpha, n)^{16}O$ cross section measurement of Brandenburg *et al.* [43] (blue points) with the sum of the three open deexcitation channels (n_0: deBoer *et al.* [45] (green squares); n_1: this work (grey lines); n_2: deBoer *et al.* [40] (yellow triangles)]. This sum and its uncertainty are represented by the orange solid and dashed lines, respectively. See text for details.

energies comes into better agreement. The $^{13}C(\alpha, n_2)^{16}O$ cross section becomes significant at ≈5.3 MeV and higher in energy. Here the differential $^{13}C(\alpha, n_2\gamma)^{16}O$ data from deBoer *et al.* [40] have been scaled by a factor of 4π to obtain an estimate of the angle integrated $^{13}C(\alpha, n_2)^{16}O$ cross section. Reasonable agreement is observed between the sum of the three partial cross sections and the total data of Brandenburg *et al.* [43] over this energy range.

VI. SUMMARY

An accurate determination of the $^{13}C(\alpha, n)^{16}O$ cross section from near the reaction threshold up to ≈9 MeV is desired for applications ranging from nuclear synthesis to energy generation to large volume neutrino and dark matter detectors. Yet there remain large portions of the cross section that are very uncertain due to a lack of measurements and reliable theory. In particular, angular distributions and partial cross sections, remain poorly, or even completely, unmeasured.

In this work, first measurements of the partial differential cross section of the $^{13}C(\alpha, n_1)^{16}O$ reaction have been made from near the reaction threshold up to 5.6 MeV using a ^{3}He neutron spectrometer. A simplified R-matrix analysis has been used to estimate the angle integrated cross section from the $\theta_{lab} = 15^\circ$ differential cross section and angular distributions at four energies. The data were compared with previous theory estimates of the $^{13}C(\alpha, n_1)^{16}O$ cross section based on statistical model calculations and show up to an order of magnitude deviation over wide energy regions. The present $^{13}C(\alpha, n_1)^{16}O$ data were then summed with other partial cross section measurements of the $^{13}C(\alpha, n_0)^{16}O$ and $^{13}C(\alpha, n_2)^{16}O$ reactions and compared to recent total reaction cross section measurements, where fair agreement was found.

While the measurements presented here represent a first step forward in the characterization of the $^{13}C(\alpha, n_1)^{16}O$ cross section, comparison with theory calculations makes it clear that further measurements are required to obtain an evaluation of the partial cross sections to the desired precision, better than 10%, up to $E_\alpha \approx 9$ MeV. To this end, new measurements of these and other (α, n) partial differential cross sections are underway at the University of Notre Dame NSL.

ACKNOWLEDGMENTS

This research utilized resources from the Notre Dame Center for Research Computing and was supported by the National Science Foundation through Grant No. Phys-2011890, and the Joint Institute for Nuclear Astrophysics through Grant No. PHY-1430152 (JINA Center for the Evolution of the Elements).

[1] D. C. Malling, S. Fiorucci, M. Pangilinan, J. J. Chapman, C. H. Faham, J. R. Verbus, and R. J. Gaitskell, Dark matter search backgrounds from primordial radionuclide chain disequilibrium, arXiv:1305.5183.

[2] D.-M. Mei, C. Zhang, and A. Hime, Evaluation of (α, n) induced neutrons as a background for dark matter experiments, Nucl. Instrum. Methods Phys. Res., Sect. A **606**, 651 (2009).

[3] B. Lehnert, Backgrounds in the DEAP-3600 dark matter experiment, J. Phys.: Conf. Ser. **1342**, 012072 (2020).

[4] D. Baxter, R. Bunker, S. Shaw, S. Westerdale, I. Arnquist, D. S. Akerib, R. Calkins, S. Cebrián, J. B. Dent, M. L. di Vacri, J. Dobson, D. Egana-Ugrinovic, A. Erlandson, C. Ghag, C. Hall, J. Hall, S. Haselschwardt, E. Hoppe, C. M. Jackson, Y. Kahn *et al.*, Snowmass2021 cosmic frontier white paper: Calibrations and backgrounds for dark matter direct detection, arXiv:2203.07623.

[5] L. Segui, *Background reduction in the SNO+ experiment*, in *Low Radioactivity Techniques 2015 (LRT 2015): Proceedings of the 5th International Workshop in Low Radioactivity Techniques*, 18–20 March 2015, Seattle, edited by J. L. Orrell, AIP Conf. Proc. No. 1672 (AIP, New York, 2015), p. 110002.

[6] S. Andringa, E. Arushanova, S. Asahi, M. Askins, D. J. Auty, A. R. Back, Z. Barnard, N. Barros, E. W. Beier, A. Bialek, S. D. Biller, E. Blucher, R. Bonventre, D. Braid, E. Caden, E. Callaghan, J. Caravaca, J. Carvalho, L. Cavalli, D. Chauhan *et al.*, Current status and future prospects of the SNO+ experiment, Adv. High Energy Phys. **2016**, 6194250 (2016).

[7] A. Gando, Y. Gando, K. Ichimura, H. Ikeda, K. Inoue, Y. Kibe, Y. Kishimoto, M. Koga, Y. Minekawa, T. Mitsui, T. Morikawa, N. Nagai, K. Nakajima, K. Nakamura, K. Narita, I. Shimizu, Y. Shimizu, J. Shirai, F. Suekane, A. Suzuki, M. P. Decowski *et al.*, (The KamLAND Collaboration), Constraints on θ_{13} from a three-flavor oscillation analysis of reactor antineutrinos at kamland, Phys. Rev. D **83**, 052002 (2011).

[8] M. Agostini, M. Allardt, E. Andreotti, A. M. Bakalyarov, M. Balata, I. Barabanov, M. B. Heider, N. Barros, L. Baudis, C. Bauer, N. Becerici-Schmidt, E. Bellotti, S. Belogurov, S. T. Belyaev, G. Benato, A. Bettini, L. Bezrukov, T. Bode, V. Brudanin, R. Brugnera *et al.*, The background in the $0\nu\beta\beta$ experiment GERDA, Eur. Phys. J. C **74**, 2764 (2014).

[9] M. J. Dolinski, A. W. P. Poon, and W. Rodejohann, Neutrinoless double-beta decay: Status and prospects, Annu. Rev. Nucl. Part. Sci. **69**, 219 (2019).

[10] T. Murata, H. Matsunobu, and K. Shibata, Evaluation of the (α, xn) reaction data for JENDL/AN-2005, JAEA-Research Report No. 2006-052, 2006 (unpublished).

[11] M. Febbraro, R. J. deBoer, S. D. Pain, R. Toomey, F. D. Becchetti, A. Boeltzig, Y. Chen, K. A. Chipps, M. Couder, K. L. Jones, E. Lamere, Q. Liu, S. Lyons, K. T. Macon, L. Morales, W. A. Peters, D. Robertson, B. C. Rasco, K. Smith, C. Seymour *et al.*, New $^{13}C(\alpha, n)^{16}O$ Cross Section with Implications for Neutrino Mixing and Geoneutrino Measurements, Phys. Rev. Lett. **125**, 062501 (2020).

[12] K. Eguchi, S. Enomoto, K. Furuno, J. Goldman, H. Hanada, H. Ikeda, K. Ikeda, K. Inoue, K. Ishihara, W. Itoh, T. Iwamoto, T. Kawaguchi, T. Kawashima, H. Kinoshita, Y. Kishimoto, M. Koga, Y. Koseki, T. Maeda, T. Mitsui, M. Motoki *et al.* (KamLAND Collaboration), First Results from KamLAND: Evidence for Reactor Antineutrino Disappearance, Phys. Rev. Lett. **90**, 021802 (2003).

[13] D. Tilley, H. Weller, and C. Cheves, Energy levels of light nuclei $A = 16$–17, Nucl. Phys. A **564**, 1 (1993).

[14] C. R. Brune, W. H. Geist, R. W. Kavanagh, and K. D. Veal, Sub-Coulomb α Transfers on ^{12}C and the $^{12}C(\alpha, \gamma)^{16}O$ S Factor, Phys. Rev. Lett. **83**, 4025 (1999).

[15] Z. Meisel, C. Brune, S. Grimes, D. Ingram, T. Massey, and A. Voinov, The Edwards Accelerator Laboratory at Ohio University, Phys. Procedia **90**, 448 (2017), Conference on the Application of Accelerators in Research and Industry, CAARI 2016, 30 October 4 November 2016, Ft. Worth, TX, USA.

[16] K. Brandenburg, The Design, Validation, and Future Plans for a New Neutron Detector at Ohio University, in *APS Division of Nuclear Physics Meeting Abstracts*, APS Meeting Abstracts (APS, Ridge, NY, 2019), Vol. 2019, p. RM.005.

[17] J. Ziegler, The Stopping and Range of Ions in Matter SRIM, 2008, www.srim.org.

[18] Bubble Technologies Industries Inc., 31278 Highway 17, P.O. Box 100, Chalk River, Ontario, Canada.

[19] H. Franz, W. Rudolph, H. Ohm, K.-L. Kratz, G. Herrmann, F. Nuh, D. Slaughter, and S. Prussin, Delayed-neutron spectroscopy with ^{3}He spectrometers, Nucl. Instrum. Methods **144**, 253 (1977).

[20] C. A. Burke, M. T. Lunnon, and H. W. Lefevre, $^7Li(p, n_0)^7Be$ angular distributions to $E_p = 3.8$ MeV, Phys. Rev. C **10**, 1299 (1974).

[21] V. V. Zerkin and B. Pritychenko, The experimental nuclear reaction data (EXFOR): Extended computer database and Web retrieval system, Nucl. Instrum. Methods Phys. Res., Sect. A **888**, 31 (2018).

[22] H. Ohm, K.-L. Kratz, and S. Prussin, The analysis of delayed neutron energy spectra recorded with ^{3}He ionization chambers, Nucl. Instrum. Methods Phys. Res., Sect. A **256**, 76 (1987).

[23] See Supplemental Material at http://link.aps.org/supplemental/10.1103/PhysRevC.106.055808 for tabulated experimental data.

[24] M. Heil, R. Detwiler, R. E. Azuma, A. Couture, J. Daly, J. Görres, F. Käppeler, R. Reifarth, P. Tischhauser, C. Ugalde, and M. Wiescher, $^{13}C(\alpha, n)$ reaction and its role as a neutron source for the s process, Phys. Rev. C **78**, 025803 (2008).

[25] R. E. Azuma, E. Uberseder, E. C. Simpson, C. R. Brune, H. Costantini, R. J. de Boer, J. Görres, M. Heil, P. J. LeBlanc, C. Ugalde, and M. Wiescher, AZURE: An R-matrix code for nuclear astrophysics, Phys. Rev. C **81**, 045805 (2010).

[26] E. Uberseder and R. J. deBoer, AZURE2 User Manual, 2015, azure.nd.edu.

[27] D. Odell, C. R. Brune, D. R. Phillips, R. J. deBoer, and S. N. Paneru, Performing Bayesian analyses with `AZURE2` using `BRICK`: An application to the ^{7}Be system, Front. Phys. **10**, 888476 (2022).

[28] C. R. Brune, Alternative parametrization of R-matrix theory, Phys. Rev. C **66**, 044611 (2002).

[29] L. Leal, E. Ivanov, G. Noguere, A. Plompen, and S. Kopecky, Resonance parameter and covariance evaluation for ^{16}O up to 6 MeV, Eur. J. Nucl. Sci. Technol. **2**, 43 (2016).

[30] S. Chakraborty, A. Mukherjee, and S. Roy, R-matrix analyses of $^{16}O(n, n)$ scattering and $^{13}C(\alpha, n)$ reaction at astrophysical energies relevant to low-mass AGB stars, Int. J. Mod. Phys. E **28**, 1950076 (2019).

[31] D. Brown, M. Chadwick, R. Capote, A. Kahler, A. Trkov, M. Herman, A. Sonzogni, Y. Danon, A. Carlson, M. Dunn, D. Smith, G. Hale, G. Arbanas, R. Arcilla, C. Bates, B. Beck, B. Becker, F. Brown, R. Casperson, J. Conlin *et al.*, ENDF/B-VIII.0: The 8th major release of the nuclear reaction data library with CIELO-project cross sections, new standards and thermal scattering data, Nucl. Data Sheets **148**, 1 (2018), Special Issue on Nuclear Reaction Data.

[32] W. Huang, G. Audi, M. Wang, F. G. Kondev, S. Naimi, and X. Xu, The AME2016 atomic mass evaluation (I). Evaluation of input data and adjustment procedures, Chin. Phys. C **41**, 030002 (2017).

[33] M. Wang, G. Audi, F. G. Kondev, W. Huang, S. Naimi, and X. Xu, The AME2016 atomic mass evaluation (II). Tables, graphs and references, Chin. Phys. C **41**, 030003 (2017).

[34] D. Foreman-Mackey, D. W. Hogg, D. Lang, and J. Goodman, emcee: The MCMC hammer, Publ. Astron. Soc. Pac. **125**, 306 (2013).

[35] P. Mohr, Revised cross section of the $^{13}C(\alpha, n)^{16}O$ reaction between 5 and 8 MeV, Phys. Rev. C **97**, 064613 (2018).

[36] T. Iguchi and Tokio Fukahor, Proceedings of the 1996 Symposium on Nuclear Data 21-22 November 1996, JAERI, Tokai, Ibaraki, Japan, https://inis.iaea.org/collection/NCLCollectionStore/_Public/28/057/28057901.pdf?r=1.

[37] A. Koning, D. Rochman, J.-C. Sublet, N. Dzysiuk, M. Fleming, and S. van der Marck, TENDL: Complete nuclear data library for innovative nuclear science and technology, Nucl. Data Sheets **155**, 1 (2019), Special Issue on Nuclear Reaction Data.

[38] J. K. Bair and F. X. Haas, Total neutron yield from the reactions $^{13}C(\alpha, n)^{16}O$ and $^{17,18}O(\alpha, n)^{20,21}Ne$, Phys. Rev. C **7**, 1356 (1973).

[39] S. Harissopulos, H. W. Becker, J. W. Hammer, A. Lagoyannis, C. Rolfs, and F. Strieder, Cross section of the $^{13}C(\alpha, n)^{16}O$ reaction: A background for the measurement of geo-neutrinos, Phys. Rev. C **72**, 062801(R) (2005).

[40] R. deBoer, M. Febbraro, D. Bardayan, K. Brandenburg, C. Brune, B. Hackett, A. Gula, G. Gyürky, R. Kelmar, K. Manukyan, S. McGuinness, Z. Meisel, L. Morales, P. Scholz, E. Stech, R. Toomey, J. Wilkinson, and M. Wiescher (unpublished).

[41] R. H. Spear, J. D. Larson, and J. D. Pearson, Excitation function for the reaction $C^{13}(\alpha, n\gamma)O^{16}$, Nucl. Phys. **41**, 353 (1963).

[42] W. A. Peters, Comment on "Cross section of the $^{13}C(\alpha, n)^{16}O$

reaction: A background for the measurement of geo-neutrinos", Phys. Rev. C **96**, 029801 (2017).

[43] K. Brandenburg, G. Hamad, Z. Meisel, C. R. Brune, D. E. Carter, R. deBoer, J. Derkin, C. Feathers, D. Ingram, Y. Jones-Alberty, B. Kenady, T. N. Massey, M. Saxena, D. Soltesza, S. K. Subedi, A. V. Voinov, J. Warren, and M. Wiescher, Measurements of the $^{13}C(\alpha, n)^{16}O$ cross section up to $E_\alpha = 8$ MeV (unpublished).

[44] P. S. Prusachenko, T. L. Bobrovsky, I. P. Bondarenko, M. V. Bokhovko, A. F. Gurbich, and V. V. Ketlerov, Measurement of the cross section for the $^{13}C\,(\alpha, n)^{16}O$ reaction and determination of the cross section for the $^{16}O\,(n, \alpha)\,^{13}C$ reaction, Phys. Rev. C **105**, 024612 (2022).

[45] R. deBoer, M. Febbraro, D. Bardayan, C. Boomershine, K. Brandenburg, C. Brune, S. Coil, J. Derkin, S. Dede, F. Fang, A. Fritsch, A. Gula, G. Gyürky, B. Hackett, G. Hamad, Y. Jones-Alberty, R. Kelmar, K. Manukyan, M. Matney, J. McDonaugh *et al.* (unpublished).

[46] E. A. Davis, T. W. Bonner, D. W. Worley, and R. Bass, Disintegration of O^{16} and C^{12} by fast neutrons, Nucl. Phys. **48**, 169 (1963).

[47] G. Giorginis, V. Khryachkov, V. Corcalciuc, and M. Kievets, The cross section of the $^{16}O(n, \alpha)\,^{13}C$ reaction in the MeV energy range, in *ND 2007: International Converence on Nuclear Data for Science and TEchnology* (EDP Sciences, Les Ulis, France, 2007), pp. 525–528.